Biochemical Pharmacology, Vol. 57, pp. 567–577, 1999.

ISSN 0006-2952/99/$–see front matter
PII S006-2952(98)00315-3

Folic Acid-Enhanced Synergy for the Combination of Trimetrexate Plus the Glycinamide Ribonucleotide Formyltransferase Inhibitor 4-[2-(2-Amino-4-oxo-4,6,7,8-tetrahydro-3*H*-pyrimidino[5,4,6][1,4]thiazin-6-yl)-(*S*)-ethyl]-2,5-thienoylamino-L-glutamic acid (AG2034)

COMPARISON ACROSS SENSITIVE AND RESISTANT HUMAN TUMOR CELL LINES

Hélène M. Faessel,† Harry K. Slocum,† Youcef M. Rustum† and William R. Greco*†‡*

*Department of Biomathematics and †Department of Experimental Therapeutics, Roswell Park Cancer Institute, Buffalo, NY 14263, U.S.A.

ABSTRACT. Folic acid (PteGlu)-enhanced intense synergy has been observed between nonpolyglutamylatable dihydrofolate reductase (DHFR) inhibitors and polyglutamylatable inhibitors of other folate-requiring enzymes, such as glycinamide ribonucleotide formyltransferase (GARFT) and thymidylate synthase. Since this phenomenon is potentially therapeutically useful, we explored its universality by examining the combined action of a DHFR inhibitor, trimetrexate (TMQ), with a GARFT inhibitor, 4-[2-(2-amino-4-oxo-4,6,7,8-tetrahydro-3*H*-pyrimidino[5,4,6][1,4]thiazin-6-yl)-(*S*)-ethyl]-2,5-thienoylamino-L-glutamic acid (AG2034), in eight human cultured cell lines. Using a 96-well plate cell growth inhibition assay, four ileocecal adenocarcinoma cell lines [HCT-8, HCT-8/DW2 (Tomudex-resistant), HCT-8/DF2 (Tomudex-/FdUrd-resistant), and HCT-8/50 (adapted to 50 nM PteGlu)], three head and neck carcinoma cell lines [A253, FaDu, and Hep-2/500 (FdUrd-resistant)], and a non-small cell lung carcinoma cell line [H460] were treated for 96 hr with TMQ + AG2034 in the presence of 2.3 or 40 μM PteGlu. Cell growth was measured with the sulforhodamine B assay at the end of this period. Drug interactions were assessed by fitting a 7-parameter model including a synergism parameter, α, to data with weighted nonlinear regression. Isobologram analysis was also applied. At 2.3 μM PteGlu, cells exhibited similar intensities of Loewe synergy for the combination of TMQ + AG2034. Loewe synergy was abolished in HCT-8/50 cells cultured and studied in 50 nM PteGlu. At 40 μM PteGlu, the intensity of the combined action in all cell lines was increased. However, the most intense Loewe synergy was seen with HCT-8, HCT-8/DF2, H460, FaDu, A253, and Hep-2/500 cells, whereas the HCT-8/50 subculture showed less of the phenomenon, and PteGlu enhancement was the least with HCT-8/DW2, a subline deficient in folylpolyglutamate synthetase (FPGS). The universality of the PteGlu-enhanced intense synergy phenomenon is suggested. Impaired FPGS activity and low-folate adaptation prior to treatment significantly lessen the degree of PteGlu enhancement. BIOCHEM PHARMACOL **57**;5:567–577, 1999. © 1999 Elsevier Science Inc.

KEY WORDS. antifolate; dihydrofolate reductase; polyglutamylation; isobol; folic acid

Because of the importance of purine nucleotides for DNA and RNA synthesis, tumor cells have been thought to be particularly vulnerable to inhibition of purine biosynthesis. This is because of their rapid growth rates and often decreased activity of purine salvage enzymes [1–3]. GARFT§ catalyzes the first of two folate-dependent reactions in *de novo* purine biosynthesis, i.e. the transfer of the formyl group of 10-CHO-$H_4PteGlu_n$ to the amino group of glycinamide ribonucleotide to form formylglycinamide ribonucleotide and $H_4PteGlu_n$. Emerging from a computerized molecular modeling study of the GARFT domain of the human trifunctional enzyme, the inhibitor AG2034 was designed to have a high affinity for the folate cofactor binding site [4]. This antipurine compound, which contains

‡ Corresponding author: Dr. W. R. Greco, Department of Biomathematics, Roswell Park Cancer Institute, Elm and Carlton Streets, Buffalo, NY 14263. Tel. (716) 845-8641; FAX (716) 845-8467; E-mail: rosgreco@acsu.buffalo.edu

¶ *Abbreviations:* GARFT, glycinamide ribonucleotide formyltransferase; SRB, sulforhodamine B; dFBS, dialyzed fetal bovine serum; MFM, minimum folate medium; DHFR, dihydrofolate reductase; TS, thymidylate synthase; TK, thymidine kinase; FPGS, folylpoly-γ-glutamate synthetase; PteGlu, folic acid; $H_2PteGlu_n$, dihydropteroylpolyglutamates; $H_4PteGlu_n$ tetrahydropteroylpolyglutamates; CH_2-$H_4PteGlu_n$, 5,10-methylenetetrahydropteroylpolyglutamates; 10-CHO-$H_4PteGlu_n$, 10-formyltetrahydropteroylpolyglutamates; mFBP, membrane folate binding protein; TMQ (trimetrexate), 2,4-diamino-5-methyl-6-[(3,4,5-trimethoxyanilino) methyl] quinazoline; AG2034, 4-[2-(2-amino-4-oxo-4,6,7,8-tetrahydro-3*H*-pyrimidino [5,4,6][1,4]thiazin-6-yl)-(*S*)-ethyl]-2,5-thienoylamino-L-glutamic acid; FdUrd, 5-fluoro-2′-deoxyuridine; Tomudex (ZD-1694), *N*- [5-[*N*-(3,4-dihydro-2-methyl-4-oxoquinazolin-6-ylmethyl)-*N*-methylamino]-2-thenoyl]-L-glutamic acid; DDATHF, [6*R*,*S*]-5,10-dideaza-5,6,7,8-tetrahydrofolate; Lometrexol (LY249543), 6*R*-DDATHF; and LY309887, [6*R*]-2′,5′-thienyl-DDATHF.

Received 26 May 1998; accepted 10 August 1998.

a terminal glutamate moiety, is also a good substrate for FPGS. Because its biochemical profile suggests an improved antitumor activity and more manageable toxicity than Lometrexol, AG2034 is being studied in a Phase I clinical trial. A congener of AG2034, LY309887, is also under active investigation [5, 6].

We extended the initial findings from other groups on the positive interaction of specific pairs of antifolates [7–11], and demonstrated in an *in vitro* HCT-8 cell system that DHFR inhibitors were capable of enhancing the growth inhibitory activity of potent polyglutamylatable TS and GARFT inhibitors, especially under very high PteGlu concentrations [12]. The concept of modulation of antifolate synergism by PteGlu was first introduced for combinations of TMQ plus 10-propargyl-5,8-dideazafolate (PDDF) or TMQ plus DDATHF with 4.6 μM PteGlu in human Manca lymphoma cells [8], and was extended later by increasing the synergy dramatically by raising medium PteGlu to 40 μM [13]. The combined action of a lipophilic DHFR inhibitor, TMQ, plus AG2034 led to the highest degree of Loewe synergism [12] ever reported in the literature, to the best of our knowledge. Therefore, we have chosen this unique interaction and a variety of human tumor cell lines to explore the universality of the phenomenon and deepen our mechanistic understanding of the synergistic process. Each of the 41 two-drug combined-action cell growth inhibition experiments reported here was rigorously quantified using the Universal Response Surface Approach (URSA) [14, 15]. Isobolograms were also examined to reveal patterns of synergism and antagonism at several effect levels.

MATERIALS AND METHODS

Drugs and Chemicals

TMQ was provided by the Parke-Davis Division, Warner Lambert Co. Tomudex was supplied by Zeneca Pharmaceuticals and AG2034 by Agouron Pharmaceuticals, Inc. PteGlu and SRB were purchased from the Sigma Chemical Co. Folate-free and "standard" RPMI 1640 (2.3 μM PteGlu) cell culture media, dFBS, and trypsin were obtained from Gibco. 6-[^{3}H]FdUMP (18 Ci/mmol) was purchased from Moravek Biochemicals, Inc. Purified *Lactobacillus casei* TS was obtained from Dr. D. G. Priest (Medical University of South Carolina). Sephadex G-25 fine was purchased from Pharmacia Biotechnology Inc.

Cell Culture and Establishment of an HCT-8 Subculture in MFM

The human HCT-8 (ileocecal adenocarcinoma) [16], A253 (epidermoid carcinoma, submaxillary gland) [17], FaDu (squamous cell carcinoma, pharynx) [18], and H460 (non-small cell lung carcinoma) [19] cell lines were obtained from the American Type Culture Collection.

Two HCT-8 sublines, made resistant to TS inhibitors, were supplied by Dr. K. Lu, Roswell Park Cancer Institute. The resistant HCT-8/DW2 subline was selected by repeated exposure of HCT-8 to escalating doses of Tomudex and exhibits decreased FPGS levels [20]. The double-resistant HCT-8/DF2 subline was established by two sequences of drug treatment, in which HCT-8 was exposed to FdUrd repeatedly, followed by Tomudex. Its degree of resistance is 130- or 75-fold relative to HCT-8 in a 2-hr exposure to Tomudex or FdUrd, respectively. Also, HCT-8/DF2 has decreased TK activity, as well as decreased *in situ* TS activity [21]. All of the cell lines were grown in RPMI 1640 medium containing 10% dFBS and 1 mM sodium pyruvate, except for the FaDu and A253 cells, which were passaged in RPMI 1640 containing 10% dFBS.

For the establishment of HCT-8 subcultures in MFM, 5×10^5 cells were seeded into 75-cm^2 flasks containing 20 mL of folate-free RPMI 1640 containing 10% dFBS. PteGlu was added to each of the four flasks 48 hr after seeding to generate the final concentrations of 200, 100, 50, and 20 nM. After 4 weeks, the cells grew with almost the same population doubling time (ranging from 20.3 to 22.7 hr) as the parent cell line (20.3 hr). These HCT-8/MFM lines were designated as HCT-8/200, HCT-8/100, HCT-8/50, and HCT-8/20, respectively. The FdUrd-resistant variant of the human laryngeal carcinoma HEp-2 cell line, HEp-2/500, was provided by Dr. S. H. Berger [22]. Cells were progressively adapted to 0.5 μM FdUrd in RPMI 1640 containing 5% horse serum, 100 μM deoxyinosine, and 10 μM folinic acid. Drug resistance was associated with an 80-fold increase in the cellular level of TS, as a result of gene amplification. HEp-2/500 was maintained further in the presence of FdUrd in RPMI 1640 containing 10% dFBS, 100 μM deoxyinosine, and 10 μM folinic acid, but was passaged twice in the absence of the TS inhibitor before use in growth inhibition assays.

Cells were maintained as monolayers in 75-cm^2 flasks incubated at 37° in a 5% CO_2 humidified atmosphere and transferred after trypsinization, twice weekly. Cell cultures were tested routinely for mycoplasma (Gen-Probe Mycoplasmas T. C.), and found negative.

Growth Inhibition Studies

A typical two-drug combined-action experiment involved a stack of five 96-well plates with five replicates of each drug treatment condition (440 total data points). Exponentially growing cells were plated at a density of 200 cells/well in 175 μL of medium, and drug treatment was initiated 24 hr after plating. Solutions of TMQ and AG2034 in medium were freshly prepared from concentrated stock solutions of 1 and 10 mM, respectively. Appropriate volumes were used to obtain the five fixed-ratio binary mixtures of TMQ plus AG2034 (1:4, 1:2, 1:1, 2:1, and 4:1) at the predicted ID_{50} values (absolute molar ratios are reported in the remainder of the paper). The agents alone and their mixtures were serially diluted over a 10^6-fold concentration range, randomly assigned to wells, and then incubated with cells for 96 hr as described by Faessel *et al.* [12]. Cell growth

inhibition was quantified by the SRB assay at the end of this period [23, 24].

Measurements of Combined CH_2-H_4PteGlu$_n$ + H_4PteGlu$_n$ Pools

The method is based upon enzymatic conversion of reduced folates to CH_2-H_4PteGlu$_n$ followed by its stoichiometric entrapment into a stable ternary complex with excess *L. casei* TS and 6-[^{3}H]FdUMP, as described previously [25]. Exponentially growing cells were trypsinized, washed twice with PBS, and frozen as cell pellets (2×10^6 cells) at −70°. Cells were extracted with 100 μL extraction buffer containing 75 mU/mL of TS and 62 nM 6-[^{3}H]FdUMP, 6.5 mM formaldehyde, 50 mM sodium ascorbate, 213 mM sucrose, 1 mM disodium-EDTA, and 50 mM Tris–HCl, pH 7.5. The reaction mixtures were incubated at 30° for 1 hr, and then boiled with 6% SDS for 3 min. Ternary complexes were separated from free 6-[^{3}H]FdUMP by centrifuging 25-μL aliquots through Sephadex G-25 minicolumns. Bound radioactivity was measured by scintillation counting. CH_2-H_4PteGlu$_n$ + H_4PteGlu$_n$ levels are expressed as picomoles per milligram of protein. Protein content in cell extracts was assayed with the Bio-Rad protein assay solution using bovine serum albumin, according to Bradford [26]. Because of a slight nonlinearity in the standard curve, a macro for curvilinear regression was run in Excel (Microsoft) to determine the amount of protein in the unknown samples.

Assessment of In Vitro *Drug Interactions*

Data from individual two-drug combination experiments were analyzed with URSA. With the assumption of the structural Hill model (Equation A) for the concentration–effect curve of each single agent, Equation B was fitted to all the data at once for each separate experiment with iteratively reweighted nonlinear regression, enabling the estimation of a synergism-antagonism parameter, α, with its standard error [14, 27]. The custom software package SYNFIT (written in FORTRAN, Microsoft Corp.) was used for the fitting procedure.

$$E = \frac{(Econ - B)\left(\frac{D}{ID_{50}}\right)^m}{1 + \left(\frac{D}{ID_{50}}\right)^m} + B \qquad \text{(A)}$$

$$1 = \frac{D_1}{ID_{50,1}\left(\frac{E - B}{Econ - E}\right)^{1/m_1}} + \frac{D_2}{ID_{50,2}\left(\frac{E - B}{Econ - E}\right)^{1/m_2}} + \frac{\alpha D_1 D_2}{ID_{50,1} ID_{50,2}\left(\frac{E - B}{Econ - E}\right)^{(1/2m_1 + 1/2m_2)}} \qquad \text{(B)}$$

E is the measured effect, and D is the drug concentration. The seven estimable parameters are: *Econ*, the control response; *B*, the background; ID_{50}, the drug concentration inducing a 50% inhibition of the maximal cell growth; and *m*, the slope parameter of the concentration–effect curve. When α is positive, Loewe synergy is indicated; when α is negative, Loewe antagonism is indicated; and when α is zero, Loewe additivity is indicated [28].

An isobologram analysis adapted from the approach of Gessner [29] was also applied to all combined-action data sets. Individual fittings of Equation A to data were performed for each growth inhibition curve for the single agents and the five constant ratio mixtures. The resulting ID_{50} estimate for each mixture was used to calculate the ID_X (X = 10, 25, 50, 75, 90) contributions for each agent in the mixture, which were then plotted on normalized isobolograms.

All graphs were made with Sigma Plot 3.0 (Jandel Scientific).

RESULTS

TMQ + AG2034 against Colon, Head and Neck, and Lung Cancer Cell Lines

Five cell lines from three different human solid tumors (colon, head and neck, and lung) were exposed for 96 hr to simultaneous combinations of TMQ and AG2034 at two different concentrations of PteGlu. Table 1 includes the ID_{50} (measure of drug potency) and α (measure of Loewe synergy) parameter estimates (± SEM) obtained from the best fit of Equation B to data from individual two-drug combined-action cell growth inhibition experiments conducted with FaDu, A253, HEp-2/500, and H460 cells. Because the two antifolates have been studied extensively alone and in combination in HCT-8 cells, geometric means for ID_{50} values and α values [± 95% confidence limits] were calculated from a total of 45 *in vitro* experiments; individual ID_{50} or α parameters were estimated by fitting Equation A or Equation B to data, respectively [12]. Each of the 2.3 μM (standard PteGlu cell culture medium level) and 40 μM PteGlu concentrations was present during the cell plating 24 hr before the drug treatment and during the entire incubation time period. Note that FaDu and HEp-2/500 cells were allowed to grow 1 extra day (120-hr drug exposure) for a suitable absorbance signal at 570 nm.

At 2.3 μM PteGlu, TMQ had a similar potency ($ID_{50,TMQ}$ = 0.852 to 3.11 nM) for 96-hr exposure against all cell lines, except FaDu ($ID_{50,TMQ}$ = 13.0 nM). Compared with an ID_{50} of 4.87 nM in HCT-8 cells, AG2034 was equipotent in H460 cells, but 2.2-, 5.3-, and 14-fold less potent in A253, HEp-2/500, and FaDu cells, respectively. As shown in Table 1, 40 μM PteGlu raised the $ID_{50,AG2034}$ 88-fold but the $ID_{50,TMQ}$ only 8.8-fold in HCT-8 cells. The protective effect of PteGlu against TMQ was also limited in other cell lines, ranging from 3- to 5-fold; and PteGlu protection of AG2034 was extreme in FaDu cells (164-fold)

TABLE 1. Estimates of the individual ID_{50} and the synergism-antagonism parameter, α, from experiments conducted in five human tumor cell lines

Human tumor cell lines	PteGlu (μM)	TMQ ID_{50}, nM	AG2034 ID_{50}, nM	Antifolate interaction	
				α*	Nature
HCT-8†	2.3	0.972 [0.847; 1.11]	4.87 [4.04; 5.05]	3.72 [3.27; 5.96]	SYN
	40	8.60 [7.24; 10.2]	427 [243; 752]	114 [84.9; 153]	SYN
FaDu‡§	2.3	13.0 ± 0.71	69.6 ± 6.8	8.53 ± 1.2*	SYN
	40	50.0 ± 3.4	11,387 ± 1,872	262 ± 48*	SYN
A253§	2.3	3.1 ± 0.18	10.9 ± 0.86	4.84 ± 0.63	SYN
	40	12.4 ± 1.4	498 ± 130	465 ± 124	SYN
	2.3	2.21 ± 0.18	10.5 ± 1.08	8.70 ± 1.5*	SYN
	40	7.45 ± 0.99	296 ± 68	155 ± 35*	SYN
HEp-2/500‡§	2.3	1.48 ± 0.20	25.9 ± 6.5	2.21 ± 0.75*	SYN
	40	9.95 ± 0.88	1,187 ± 146	114 ± 15*	SYN
H460§	2.3	1.04 ± 0.023	4.39 ± 0.089	0.697 ± 0.087*	SYN
	40	5.54 ± 0.21	136 ± 21	211 ± 14*	SYN
	2.3	1.22 ± 0.021	5.00 ± 0.045	−0.195 ± 0.063	ANT
	40	6.32 ± 0.24	186 ± 9.1	160 ± 10	SYN
	2.3	0.852 ± 0.048	4.62 ± 0.22	1.48 ± 0.23	SYN
	40	5.04 ± 0.34	202 ± 21	130 ± 15	SYN

Cells were exposed for 96 hr to the TMQ + AG2034 combination in the presence of 2.3 or 40 μM PteGlu. SYN indicates Loewe synergy and ANT Loewe antagonism.

*The values refer to the TMQ + AG2034 combinations for which 2-D-isobol families are presented in Fig. 2.

†Geometric means for ID_{50} estimates with [95% confidence limits] were estimated from 43 single data sets for TMQ (32 sets at 2.3 μM PteGlu and 11 at 40 μM PteGlu) and 26 single data sets for AG2034 (21 sets at 2.3 μM PteGlu and 5 at 40 μM PteGlu); individual estimates were obtained by fitting Equation A to data. Geometric means for α estimates with [95% confidence limits] were calculated from 12 combination data sets (7 sets at 2.3 μM PteGlu and 5 at 40 μM PteGlu); individual estimates were obtained by fitting Equation B to the data.

‡Cells were incubated with TMQ + AG2034 for 120 hr.

§The listed parameter estimates (± SEM) for all cell lines, except HCT-8, were obtained by fitting Equation B to data from individual combined-action experiments. The separate results from replicate experiments are listed for A253 and H460.

and high in H460, A253, and HEp-2/500 cells (from 28- to 46-fold).

Positive α values of 2.21 to 8.70 for the HCT-8, FaDu, A253, and HEp-2/500 cell lines indicated substantial Loewe synergy at 2.3 μM PteGlu when AG2034 was combined simultaneously for 96 hr with TMQ. In the H460 non-small cell lung carcinoma cell line, two out of the three combined-action experiments showed slight Loewe synergy ($\alpha = 0.697 \pm 0.087$; $\alpha = 1.48 \pm 0.23$); once slight Loewe antagonism was observed ($\alpha = -0.195 \pm 0.063$). Raising the PteGlu level in the medium to 40 μM enhanced greatly the synergistic intensity of these TMQ + AG2034 combined actions. The relative increase in α values was more pronounced in H460 (up to 300-fold) and A253 (up to 96-fold) cells than in HEp-2/500 (52-fold), FaDu (31-fold), or HCT-8 (28-fold) cells.

TMQ + AG2034 against the HCT-8 Ileocecal Cell Line and Derived Sublines

By adapting HCT-8 cells to 200, 100, 50, and 20 nM PteGlu concentrations, we obtained the four respective sublines HCT-8/200, HCT-8/100, HCT-8/50, and HCT-8/20. These cell lines were created to provide a model closer to the normal human physiological condition of 5–30 nM plasma folates [30, 31]. A preliminary growth experiment showed that a seeding density of 200 cells/well for each subline resulted in exponential growth kinetics for at least 5 days with a mean doubling time of 21.7 hr. The measurement of the intracellular combined pool of CH_2-$H_4PteGlu_n$ + $H_4PteGlu_n$ (pmol/mg protein ± SEM) showed that adaptation of cells to low folate levels caused a sharp depletion of 6-fold in HCT-8/200 (11 ± 0.3) and HCT-8/100 (9.4 ± 1.5) cells followed by an extra 2-fold decrease in HCT-8/50 (5.3 ± 0.3) and HCT-8/20 (5.0 ± 0.02) cells, as compared with the parental HCT-8 line (65 ± 0.4).

Table 2 presents changes in drug potency (ID_{50}, geometric means) and slope parameter (*m*, arithmetic means) estimates with PteGlu when HCT-8 cells and three sublines were exposed for 96 hr to the single agents TMQ or AG2034. Each of the 185 single-agent data sets included a total of 110 data points with 55 controls and 5 replicates for each of 11 serial drug dilutions. Equation A was fit to each individual data set, and *Econ*, ID_{50}, *m*, and *B* were estimated. At 2.3 μM PteGlu, the HCT-8/DW2 subline was 2.9-fold more sensitive to TMQ, but 7.6-fold more resistant to AG2034, as compared with the parental line. HCT-8/DF2 cells were more resistant to both TMQ and AG2034 by a factor of 1.6 and 14, respectively. For HCT-8/50 cells cultured in 50 nM PteGlu, the growth inhibitory activity of

TABLE 2. Geometric means for ID_{50} estimates and arithmetic means for slope parameter (m) estimates with [95% confidence limits]

Antifolate	Cell lines	PteGlu (μM)	ID_{50} (nM)	Slope parameter, m
TMQ	HCT-8*	2.3	0.972 [0.847; 1.11]	−1.49 [−1.38; −1.60]
		40	8.60 [7.24; 10.2]	−1.66 [−1.55; −1.78]
		78	9.04 [8.01; 10.5]	−1.94 [−1.78; −2.09]
	HCT-8/DW2	2.3	0.331 [0.273; 0.403]	−1.45 [−1.37; −1.53]
		40	1.44 [1.14; 1.82]	−1.50 [−1.39; −1.61]
		78	2.00 [1.39; 2.89]	−1.66 [−1.43; −1.89]
	HCT-8/DF2	2.3	1.59 [1.45; 1.74]	−1.25 [−1.16; −1.35]
		40	8.49 [7.13; 10.1]	−1.64 [−1.47; −1.82]
	HCT-8/50	0.05	0.062 [0.015; 0.25]	−0.985 [−0.738; −1.23]
		2.3	1.07 [0.708; 1.62]	−1.49 [−1.21; −1.78]
		40	6.70 [4.04; 11.1]	−2.06 [−1.35; −2.77]
AG2034	HCT-8*	2.3	4.87 [4.04; 5.05]	−1.70 [−1.58; −1.83]
		40	427 [243; 752]	−1.19 [−1.14; −1.25]
		78	541 [452; 648]	−1.34 [−1.22; −1.46]
	HCT-8/DW2	2.3	36.9 [29.3; 46.5]	−1.72 [−1.55; −1.89]
		40	415 [361; 478]	−1.61 [−1.49; −1.72]
		78	1,357 [792; 2,326]	−1.72 [−1.54; −1.90]
	HCT-8/DF2	2.3	66.4 [21.0; 210]	−1.22 [−0.653; −1.78]
		40	2,905 [2,144; 3,936]	−1.07 [−0.313; −1.84]
	HCT-8/50	0.05	0.909 [0.471; 1.75]	−3.38 [−2.83; −3.93]
		2.3	4.31 [2.00; 9.30]	−2.17 [−1.20; −3.14]
		40	175 [87.0; 354]	−1.32 [−1.12; −1.51]

Cells from the human ileocecal HCT-8 cell line and its resistant HCT-8DW2 and HCT-8DF2 and established HCT-8/50 sublines were exposed for 96 hr to the drug in the presence of 0.05, 2.3, 40, or 78 μM PteGlu. Individual estimates were obtained by fitting Equation A to the data.

*Individual data for TMQ and AG2034 in HCT-8/WT were previously disclosed [12].

each antifolate was increased, as compared with HCT-8. A 16- and a 6-fold increase in potency were observed for TMQ and AG2034, respectively, when reducing PteGlu from 2.3 μM to 50 nM (46-fold reduction). Increasing the cell culture medium PteGlu levels reduced significantly the growth inhibitory effects of both TMQ and AG2034 in the resistant HCT-8/DW2 and HCT-8/DF2 cells, as well as the adapted HCT-8/50 cells. At 40 μM PteGlu, the $ID_{50,TMQ}$ was raised 5-fold in both HCT-8/DW2 and HCT-8/DF2 sublines, whereas the $ID_{50,AG2034}$ was raised 44-fold in HCT-8/DF2 and only 11-fold in HCT-8/DW2. For the HCT-8/50 subline, the drug potencies were decreased 17- and 6.3-fold for TMQ and 4.3- and 41-fold for AG2034 by increasing PteGlu to 2.3 and 40 μM, respectively.

We found that the Hill model, Equation A, was appropriate for all growth inhibition curves in this study. If cells are assumed to be similar in enzyme activities, signal transduction activities, cell cycle phase, and other critical characteristics, then the sigmoidal shape of a growth inhibition concentration–effect curve could be attributed to important cellular mass-action phenomena such as the gradual saturation of target enzymes or the control of enzymatic or signal transduction pathways. However, since it is well known that cultured cells within a population are heterogeneous with regard to many attributes (including cell cycle phase), the steepness of a concentration–effect curve more likely reflects a cumulative cellular tolerance distribution to a drug, which is the result of many contributors to apparent cell growth inhibition (e.g. cell killing, cell growth slow-down, and sterile daughter cells). A smaller absolute value of m (shallower slope) implies more cellular heterogeneity, and vice versa. The m estimates for TMQ clearly increased with increasing PteGlu in HCT-8, HCT-8/DF2, and HCT-8/50 cells, whereas there was a systematic diminishing trend of m_{AG2034} in HCT-8/WT and HCT-8/50 cells as PteGlu was increased; for HCT-8/DW2 cells, the slope of the concentration–effect curves for TMQ and AG2034 was not obviously altered by high folate conditions.

Figure 1 shows estimates of the synergism-antagonism parameter ($\alpha \pm 95\%$ confidence intervals, logarithmic scale) from 41 combined-action experiments, in which HCT-8 cells and four sublines were exposed simultaneously to TMQ, AG2034, and PteGlu for 96 hr. At 2.3 μM PteGlu, HCT-8/DW2 or HCT-8/DF2 cells produced an extent of Loewe synergism similar to HCT-8/WT. The combination of TMQ + AG2034 showed slight Loewe

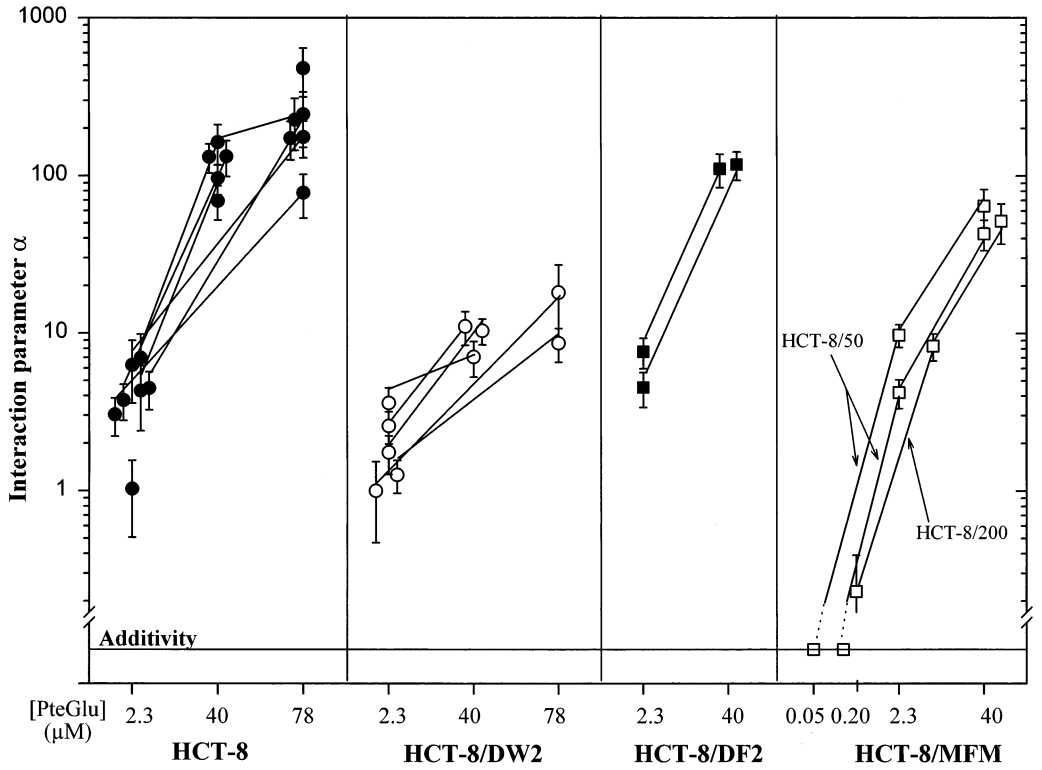

FIG. 1. Estimates of the synergism-antagonism parameter (α ± 95% confidence interval, log scale) obtained by fitting Equation B to the full data set from individual TMQ + AG2034 combination experiments with weighted nonlinear regression. Human ileocecal HCT-8/WT cells and the three sublines were exposed continuously for 96-hr to the combination in the presence of PteGlu (50 nM, 200 nM, 2.3 μM, 40 μM, or 78 μM). Each data point is from a separate 96-well plate growth inhibition assay; symbols stand for cell type: HCT-8/WT (closed circle), HCT-8/DW2 (open circle), HCT-8/DF2 (closed square), and HCT-8/MFM (open square). Solid lines link experiments done side-by-side in minimum, low, and high folate conditions. The horizontal solid line near the bottom of the figure indicates Loewe additivity. The data points on the additivity line indicate that the 95% confidence intervals for α encompassed zero.

synergy (α = 0.234 ± 0.16) in HCT-8/200 cells with 200 nM PteGlu in the medium and Loewe additivity (95% limits for α encompassed zero) in HCT-8/50 cells with 50 nM PteGlu in the medium.

High medium folate levels enhanced the combined effect of TMQ + AG2034 in all of the HCT-8 cell lines. When these cells were incubated for 24 hr with higher PteGlu levels, the size of the intracellular CH_2-$H_4PteGlu_n$ + $H_4PteGlu_n$ pool (pmol/mg protein ± SEM) increased about 2-fold for HCT-8 (from 106 ± 2 to 182 ± 4 at 40 μM PteGlu), HCT-8/DW2 (from 28 ± 0.3 to 59 ± 0.4 at 40 μM PteGlu), and HCT-8/200 (from 30 ± 0.1 to 69 ± 0.3 at 2.3 μM PteGlu and to 141 ± 0.8 at 40 μM PteGlu). The degree of antifolate synergism caused by 40 μM PteGlu was not identical in the five HCT-8 cell lines of this study (Fig. 1). The largest PteGlu-enhanced synergies were observed in HCT-8 and HCT-8/DF2 cells with α values ranging from 69 to 163 for HCT-8 and from 111 to 118 for HCT-8/DF2. PteGlu enhancement was the most limited with the HCT-8/DW2 subline for which α values ranged from 0.999 at 2.3 μM PteGlu to 11.03 at 40 μM PteGlu and to 18.1 at 78 μM PteGlu. With the HCT-8/200 and HCT-8/50 sublines, the enhancing effect of PteGlu for the TMQ + AG2034 interaction was more dramatic over the 0.05 to 2.3 μM PteGlu range than over the 2.3 to 40 μM PteGlu range; α values at 40 μM PteGlu were 53.9 for HCT-8/200, and were 64.5 and 45.6 for HCT-8/50.

Isobolographic Analyses

For a better characterization of these TMQ + AG2034 interaction surfaces, each experiment was explored through isobolographic examination. 2-D-isobol families for each cell line and PteGlu concentration are plotted in Figs. 2 and 3. Each data point is the estimated ID_X (X = 10, 25, 50, 75, 90) normalized by division by the respective ID_X of TMQ or AG2034 when given alone, as described in Materials and Methods. At 2.3 μM PteGlu, isobols for the 10, 25, and 50% effect levels contained local Loewe synergy for low concentrations of TMQ and local Loewe antagonism for intermediate and high concentrations of TMQ. These regions moved to the left toward synergy as the ID_X changed from ID_{10} to ID_{90}. Similar isobolographic behavior was observed with all other cell lines tested, except for the HCT-8/DW2 subline. This latter exhibited a near perfect Loewe synergistic ID_{10} isobol with small movements at higher effect levels. HCT-8/50 cells displayed a pure Loewe

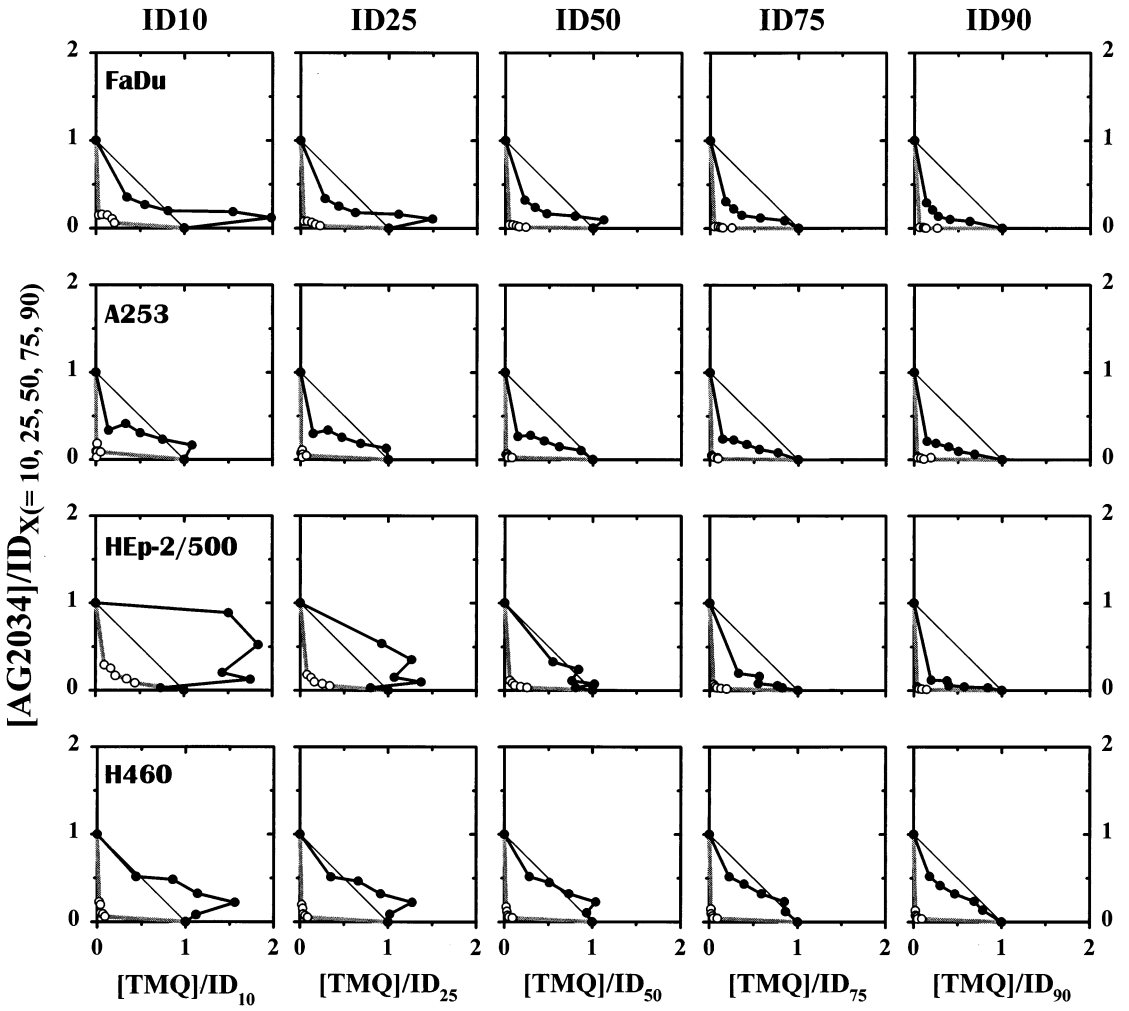

FIG. 2. Families of 2-D isobols for a 96-hr continuous exposure of four different human tumor cell lines (non-small cell lung H460 and head and neck Hep-2/500, FaDu, and A253 carcinomas) to the TMQ + AG2034 combination in RPMI 1640 10% dFBS supplemented with 2.3 μM (●) or 40 μM (○) PteGlu. For each single agent and for each constant ratio of TMQ:AG2034 (1:4, 1:2, 1:1, 2:1, and 4:1), data were fitted by Equation A, and *Econ*, *B*, ID_{50}, and *m* were estimated. The solid lines connect the points; they do not represent a fitted model. The diagonal straight lines are the Loewe additivity lines. One representative experiment for each of four cell lines is shown.

antagonistic curve at 50 nM PteGlu, collapsing toward the additivity line as the effect level increased.

At 40 μM PteGlu, seven out of the eight isobol sets became symmetrical and pressed to the origin corner of the isobologram. These are the combinations of TMQ + AG2034 that demonstrated PteGlu-enhanced intense Loewe synergies. A lesser degree of bowing of the isobols was seen for HCT-8/DW2, which is consistent with less of the Loewe synergy phenomenon and a smaller synergism parameter estimate ($\alpha = 10.4 \pm 0.97$).

DISCUSSION

In this report, we have explored the PteGlu-enhanced combined effect of the lipophilic DHFR inhibitor TMQ plus the specific GARFT inhibitor AG2034 on the growth inhibition of eight human carcinoma cell lines having differences in: (a) histologic origin (ileocecal, head and neck, and lung); (b) mechanisms of acquired resistance to the TS inhibitors FdUrd and/or Tomudex; and (c) adaptation to low medium PteGlu levels. Both isobolograms and three-dimensional concentration–effect surfaces were used to characterize rigorously the nature and the intensity of this unique *in vitro* antifolate interaction.

Collateral sensitivity to antifolates has already been described by some authors [32, 33] and associated with impaired reduced folate carrier (RFC) [34–37] or impaired FPGS activity [38]. TMQ had greater antitumor activity against the FPGS-deficient HCT-8/DW2 subline (Table 2). Work from our laboratory showed that the mechanism was related to a reduction of the intracellular reduced folate pools in the HCT-8/DW2 subline [39]. Similarly, the profound reduction in the intracellular amount of CH_2-$H_4PteGlu_n$ + $H_4PteGlu_n$ caused by folate deprivation increased the cellular sensitivity of HCT-8/50 cells to TMQ and AG2034. Similar enhancements of growth inhibitory

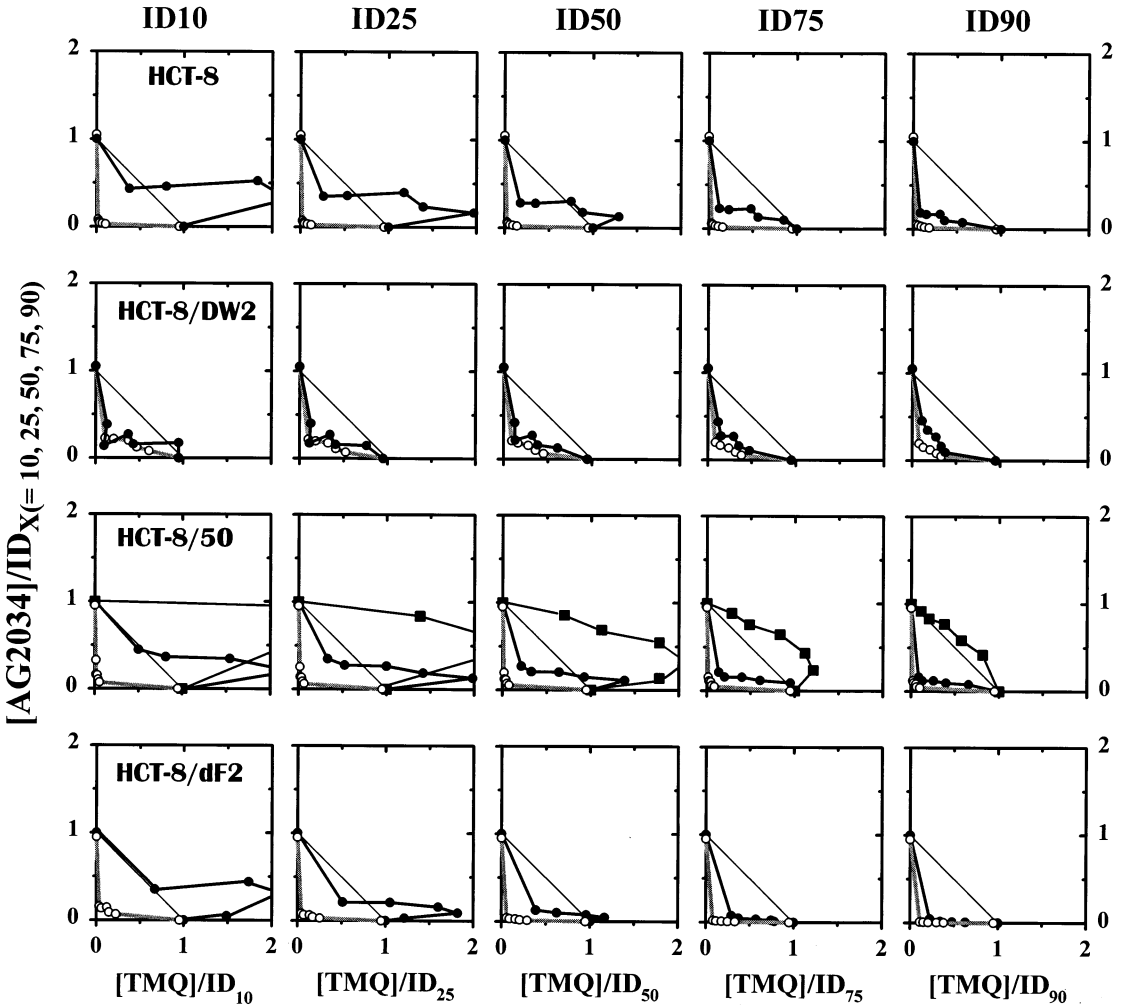

FIG. 3. Families of 2-D isobols for a 96-hr continuous exposure of human ileocecal adenocarcinoma HCT-8/WT, HCT-8/DW2, HCT-8/50, and HCT-8/DF2 cells to the TMQ + AG2034 combination in RPMI 1640 10% dFBS supplemented with 50 nM (■), 2.3 μM (●), or 40 μM (○) PteGlu. For each single agent and for each constant ratio of TMQ:AG2034 (1:4, 1:2, 1:1, 2:1, and 4:1), data were fitted by Equation A, and *Econ*, *B*, ID_{50}, and *m* were estimated. The solid lines connect the points; they do not represent a fitted model. The diagonal straight lines are the Loewe additivity lines. One representative experiment for each of four cell lines is shown.

effects for AG2034 were reported with L1210/C1920 cells at 200 nM PteGlu and HeLa S3 cells at 50 nM PteGlu [4]. An up-regulation of mFBP in these cell lines was suggested. Also, collateral sensitivity to the GARFT inhibitor DDATHF was found with head and neck cells grown in low folates on the basis of a diminished availability of extracellular folates, which can compete at sites for cellular processes [40].

All the tumor cells exhibited substantial Loewe synergy at 2.3 μM PteGlu with α values ranging from 0.999 to 9.77 for a 96-hr exposure to the TMQ + AG2034 combination. When testing the antifolate combination in HCT-8/MFM cells maintained in low PteGlu conditions, Loewe synergy was minimized in HCT-8/200 cells and absent in HCT-8/50 cells. When raising PteGlu to higher extracellular concentrations, the intensity of the TMQ + AG2034 combination was enhanced in all the cell lines tested, except for HCT-8/DW2. High Loewe synergies ($\alpha > 100$) were observed for the ileocecal HCT-8/WT and HCT-8/DF2 lines, the head and neck A253, FaDu, and Hep-2/500 lines, and the non-small cell lung H460 line. The HCT-8/50 and HCT-8/200 subcultures showed less of the phenomenon with α estimates of 45.6 to 64.5. The FPGS-deficient HCT-8/DW2 subline showed the weakest PteGlu-enhanced Loewe synergy phenomenon. Finally, changes in isobol patterns were similar for cell lines that demonstrated substantial Loewe synergy at 2.3 μM PteGlu and intense PteGlu-enhanced Loewe synergy at higher folates (Figs. 2 and 3). In contrast, there was a lesser degree of bowing of the isobols at 40 μM PteGlu for HCT-8/DW2, and isobolograms for HCT-8/50 at 50 nM PteGlu displayed Loewe antagonism at all effect levels, which was consistent with the fit of the global interaction model (Table 1 and Fig. 1).

This panel of combined-action growth inhibition experiments extends a previous report [12] on the PteGlu-enhanced Loewe synergy of a DHFR inhibitor plus another

inhibitor of a folate-dependent enzyme initially observed by Kisliuk *et al*. [7]. A reasonable explanation was that TMQ blocks the protection by PteGlu of the second inhibitor for which polyglutamylation enhances binding to its target enzyme [41]. Inhibition of DHFR blocks recycling of H_2PteGlu to H_4PteGlu$_n$ and the conversion of PteGlu to H_2PteGlu$_n$, thus depleting cells of folate cofactors that can compete with the second inhibitor for polyglutamylation and binding. Because the conversion of PteGlu to H_2PteGlu appears to be a critical step [12], high extracellular PteGlu concentrations would be expected to intensify the difference between the DHFR-inhibited state and the DHFR-uninhibited state for reduced folate inhibition of antifolate polyglutamylation.

The general finding of synergistic growth inhibition by the antifolate combination of TMQ + AG2034, along with PteGlu modulation, suggests that many kinds of mammalian cancer cells share common regulatory elements for the folate metabolic pathways. In this study, the cell lines that displayed a similar pattern of PteGlu enhancement have the intrinsic capacity to form polyglutamate derivatives. This has been shown to be true for HCT-8 [20, 42], H460 [4], and FaDu and A253 [43–45]. The critical role of polyglutamylation is further indicated when 40 μM PteGlu incubated with the FPGS-deficient HCT-8/DW2 subline was 8-fold (Table 1) more limited in reversing the growth inhibitory activity of AG2034 and 6-fold (Fig. 1) less effective in enhancing the Loewe synergy of TMQ + AG2034 than with the parental HCT-8 line. Also, higher PteGlu levels did not affect the steepness of the concentration–effect slopes for TMQ or AG2034, indicating that a factor that induced heterogeneity in drug response in other cell lines was less abundant in HCT-8/DW2 cells. Cellular differences in FPGS content/activity for changes in the pharmacodynamic profiles of both antifolates are suggested.

Several observations suggest that the PteGlu-enhanced combined action of TMQ plus AG2034 depends upon folate status prior to the application of the drug combination: (a) substantial Loewe synergy was found at 2.3 μM PteGlu in all cell lines including the HCT-8/DW2 subline. If, at the same time, less polyglutamates of AG2034 are synthesized and less folate cofactors are available, TMQ appears to effectively synergize with AG2034; (b) no Loewe synergy was present in HCT-8/50 cells cultured in 50 nM PteGlu, and the intensity of synergism brought about by 40 μM PteGlu was 2-fold lower than in the parental line. It has been reported that FPGS activity remained stable [40] or increased [40, 46, 47] in cell lines or tumors grown in low folate conditions. An increase in FPGS activity is not consistent with the absence of increased Loewe synergy in HCT-8/50 or HCT-8/200 cells relative to HCT-8 cells under 2.3 or 40 μM PteGlu. It is also known that cells exhibit a greater uptake and retention of exogenous folates under folate deprivation [48]. Because folate cofactors are better substrates for FPGS than antifolates [49], their metabolism may predominate and block, with the elongation of the chain length, the access of FPGS to polyglutamylatable antifolates [50, 51]. Another possibility is that PteGlu prevents uptake of AG2034, since AG2034 and PteGlu use mFBP as an alternative transport route [4, 52], which was shown to be up-regulated markedly by low folate conditions in a variety of human cell lines [47, 53].

The hypothesis of a differential blockage of antifolate uptake by PteGlu was not included in our mechanistic explanation for the PteGlu-enhanced synergy phenomenon [12]. The fact that Galivan's group found synergistic growth inhibitory effects for the combination of DDATHF plus TMQ or plus metoprine in a methotrexate-resistant cell line with transport defect [10] argues against RFC as a major factor for the phenomenon. However, it is very difficult to tease out polyglutamylation effects from transport competition for explaining diminished drug accumulation. Direct drug uptake studies will be useful for assessing the role of transport for this phenomenon.

In summary, using a broad spectrum of sensitive and resistant carcinoma cell lines, we report here on the universality of the synergistic growth inhibition by the combination of TMQ plus AG2034. Loewe synergy was abolished in folate-depleted cells. Enhancement of the Loewe synergy phenomenon by extracellular high PteGlu concentrations occurred in all FPGS competent cells. *In vivo* studies of the combination of TMQ + AG2034 against human tumor xenografts in nude mice are ongoing.

We thank Dr. Kun Lu for providing excellent guidance for the reduced folate pool assays and for helpful discussions, and Drs. J. J. McGuire and T. J. Boritzki for critical reviews of the manuscript. This work was supported by NIH Grants RR10742, CA16056, and CA65761, and the American Cancer Society Grant DHP178.

References

1. Jackson RC and Harkrader RJ, The contributions of *de novo* and salvage pathways of nucleotide biosynthesis in normal and malignant cells. In: *Nucleosides and Cancer Treatment* (Eds. Tattersall MHN and Fox RM), pp. 18–31. Academic Press, Sydney, 1981.
2. Ahmed NK, Haggitt RC and Welch AD, Enzymes of salvage and *de novo* pathways of synthesis of pyrimidine nucleotides in human colorectal adenocarcinomas. *Biochem Pharmacol* **31:** 2485–2488, 1982.
3. Denton JE, Lui MS, Aoki T, Sebolt J, Takeda E, Eble JN, Glover JL and Weber G, Enzymology of pyrimidine and carbohydrate metabolism in human colon carcinomas. *Cancer Res* **42:** 1176–1183, 1982.
4. Boritzki TJ, Bartlett CA, Zhang C, Howland EF, Margosiak SA, Palmer CL, Romines WH and Jackson RC, AG2034: A novel inhibitor of glycinamide ribonucleotide formyltransferase. *Invest New Drugs* **14:** 295–303, 1996.
5. Worzella JF, Self TD, Theobald KS, Rutherford PG, Gossett LS, Shih C and Mendelsohn LG, Antitumor therapeutic index of LY309887 is improved with increased folic acid supplementation in mice maintained on a folate deficient diet. *Proc Am Assoc Cancer Res* **37:** 2617, 1996.
6. Mendelsohn LG, Shih C, Schultz RM and Worzella JF, Biochemistry and pharmacology of glycinamide ribonucle-

otide formyltransferase inhibitors: LY309887 and Lometrexol. *Invest New Drugs* **14:** 287–294, 1996.
7. Kisliuk RL, Gaumont Y, Kumar P, Coutts M, Nair MG, Nanavati NT and Kalman TI, The effect of polyglutamylation on the inhibitory activity of folate analogs. In: *Proceedings of the Second Workshop on Folyl and Antifolyl Polyglutamates* (Ed. Goldman ID), pp. 319–328. Praeger, New York, 1985.
8. Kisliuk RL, Gaumont Y, Powers JF, Thorndike J, Nair MG and Piper JR, Synergistic growth inhibition by combination of antifolates. In: *Evaluation of Folate Metabolism in Health and Disease* (Eds. Picciano MF, Stokstad ELR and Gregory JF III), pp. 79–89. Alan R. Liss, New York, 1990.
9. Galivan J, Nimec Z and Rhee M, Synergistic growth inhibition of rat hepatoma cells exposed *in vitro* to N^{10}-propargyl-5,8-dideazafolate with methotrexate or the lipophilic antifolates trimetrexate or metoprine. *Cancer Res* **47:** 5256–5260, 1987.
10. Galivan J, Nimec Z, Rhee M, Boschelli D, Oronsky AL and Kerwar SS, Antifolate drug interactions: Enhancement of growth inhibition due to the antipurine 5,10-dideazatetrahydrofolic acid by the lipophilic dihydrofolate reductase inhibitors metoprine and trimetrexate. *Cancer Res* **48:** 2421–2425, 1988.
11. Gaumont Y, Kisliuk RL, Embey R, Piper JR and Nair MG, Folate enhancement of antifolate synergism in human lymphoma cells. In: *Chemistry and Biology of Pteridines* (Eds. Curtius HC, Blau N and Ghisla S), pp. 1132–1136. W. de Gruyter, Berlin, 1990.
12. Faessel HM, Slocum HK, Jackson RC, Boritzki TJ, Rustum YM, Nair MG and Greco WR, Super *in vitro* synergy between inhibitors of dihydrofolate reductase and inhibitors of other folate-requiring enzymes: The critical role of polyglutamylation. *Cancer Res* **58:** 3036–3050, 1998.
13. Gaumont Y, Kisliuk RL, Parsons JC and Greco WR, Quantitation of folic acid enhancement of antifolate synergism. *Cancer Res* **25:** 2228–2235, 1992.
14. Greco WR, Park HS and Rustum YM, Application of a new approach for the quantitation of drug synergism to the combination of *cis*-diamminedichloroplatinum and 1-β-D-arabinofuranosylcytosine. *Cancer Res* **50:** 5318–5327, 1990.
15. Greco WR, Bravo G and Parsons JC, The search for synergy: A critical review from a response surface perspective. *Pharmacol Rev* **47:** 331–385, 1995.
16. Tompkins WA, Watrach A, Schmale J, Schultz R and Harris J, Cultural and antigenic properties of newly established cell strains derived from adenocarcinomas of the human colon and rectum. *J Natl Cancer Inst* **52:** 117–133, 1974.
17. Giard DJ, Aaronson SA, Todaro GJ, Kersey JH, Dosik H and Parks WP, *In vitro* cultivation of human tumors: Establishment of cell lines derived from a series of solid tumors. *J Natl Cancer Inst* **51:** 1417–1423, 1973.
18. Rangan SRS, A new human cell line (FaDu) from a hypopharyngeal carcinoma. *Cancer* **29:** 117–121, 1972.
19. O'Connor PM, Jackman J, Bae I, Myers TG, Fan S, Mutoh M, Scudiero DA, Monks A, Sausville EA, Weinstein JN, Friend S, Fornace AJ Jr. and Kohn KW, Characterization of the p53 tumor suppressor pathway in cell lines of the National Cancer Institute Anticancer Drug Screen and correlations with the growth-inhibitory potency of 123 anticancer agents. *Cancer Res* **57:** 4285–4300, 1997.
20. Lu K, Yin M, McGuire JJ, Bonmassar E and Rustum YM, Mechanisms of resistance to *N*-[5-[*N*-(3,4-dihydro-2-methyl-4-oxoquinazolin-6-ylmethyl)-*N*-methylamino]-2-thenoyl]-L-glutamic acid (ZD1694), a folate-based thymidylate synthase inhibitor, in the HCT-8 human ileocecal adenocarcinoma cell line. *Biochem Pharmacol* **50:** 391–398, 1995.
21. Dolnick BJ, Lu K, Yin M and Rustum YM, Recent advances in the study of rTS proteins. rTS expression during growth and in response to thymidylate synthase inhibitors in human tumor cells. *Adv Enzyme Regul* **37:** 95–109, 1997.
22. Berger SH, Jenh C, Johnson LF and Berger FG, Thymidylate synthase overproduction and gene amplification in fluorodeoxyuridine-resistant human cells. *Mol Pharmacol* **28:** 461–467, 1985.
23. Rubinstein LV, Shoemaker RH, Paull KD, Simon RM, Tosini S, Skehan P, Scudiero DA, Monks A and Boyd MR, Comparison of *in vitro* anticancer-drug screening data generated with a tetrazolium assay versus a protein assay against a diverse panel of human tumor cell lines. *J Natl Cancer Inst* **82:** 1113–1118, 1990.
24. Skehan P, Storeng R, Scudiero D, Monks A, McMahon J, Vistica D, Warren JT, Bokesch H, Kenney S and Boyd MR, New colorimetric cytotoxicity assay for anticancer-drug screening. *J Natl Cancer Inst* **82:** 1107–1112, 1990.
25. Priest DG and Doig MT, Tissue folate polyglutamate chain-length determination by electrophoresis as thymidylate synthase-fluorodeoxyuridylate ternary complexes. *Methods Enzymol* **122:** 313–319, 1986.
26. Bradford MM, A rapid and sensitive method for the quantitation of microgram quantities of protein utilizing the principle of protein-dye binding. *Anal Biochem* **72:** 248–254, 1976.
27. Levasseur L, Faessel H, Slocum HK and Greco WR, Precision and pattern in 96-well plate cell growth experiments. *Proc Am Stat Assoc (Biopharm Section)* 227–232, 1995.
28. Greco WR, Unkelbach HD, Pöch G, Sühnel J, Kundi M and Bödeker W, Consensus on concepts and terminology for interaction assessment: The Saaresilkä Agreement. *Arch Complex Environ Studies* **4:** 65–69, 1992.
29. Gessner PK, The isobolographic method applied to drug interactions. In: *Drug Interactions* (Eds. Morselli PL, Garattini S and Cohen SN), pp. 349–362. Raven Press, New York, 1974.
30. Antony AC, The biological chemistry of folate receptors. *Blood* **79:** 2807–2820, 1992.
31. Kane MA and Waxman S, Biology of disease: Role of folate binding proteins in folate metabolism. *Lab Invest* **60:** 737–746, 1989.
32. Romanini A, Sobrero AF, Chou T, Sherwood RF and Bertino JR, Enhancement of trimetrexate cytotoxicity *in vitro* and *in vivo* by carboxypeptidase G_2. *Cancer Res* **49:** 6019–6023, 1989.
33. Takemura Y, Gibson W, Kimbell R, Kobayashi H, Miyachi H and Jackman AL, Cellular pharmacokinetics of ZD1694 in cultured human leukaemia cells sensitive, or made resistant, to this drug. *J Cancer Res Clin Oncol* **122:** 109–117, 1996.
34. Kano Y, Ohnuma T and Holland JF, Folate requirements of methotrexate-resistant human acute lymphoblastic leukemia cell lines. *Blood* **68:** 586–591, 1986.
35. Ohnoshi T, Ohnuma T, Takahashi I, Scanlon K, Kamen BA and Holland JF, Establishment of methotrexate-resistant human acute lymphoblastic leukemia cells in culture and effects of folate antagonists. *Cancer Res* **42:** 1655–1660, 1982.
36. Sirotnak FM, Moccio DM, Goutas LJ, Kelleher LE and Montgomery JA, Biochemical correlates of responsiveness and collateral sensitivity of some methotrexate-resistant murine tumors to the lipophilic antifolate, metoprine. *Cancer Res* **42:** 924–928, 1982.
37. van der Veer LJ, Westerhof GR, Rijksen G, Schornagel JH and Jansen G, Cytotoxicity of methotrexate and trimetrexate and its reversal by folinic acid in human leukemic CCRF-CEM cells with carrier-mediated and receptor-mediated folate uptake. *Leuk Res* **13:** 981–987, 1989.
38. McGuire JJ, Heitzman KJ, Haile WH, Russell CA, McCloskey DE and Piper JR, Cross-resistance studies of folylpolyglutamate synthetase-deficient, methotrexate-resistant CCRF-

CEM human leukemia sublines. *Leukemia* **7:** 1996–2003, 1993.
39. Lu K, Faessel HM, Slocum HK, Greco WR and Rustum YM, Role of intracellular reduced folate pools on cellular sensitivity to trimetrexate (TMQ) and methotrexate (MTX) in a folypolyglutamate synthetase (FPGS)-deficient HCT-8 subline. *Proc Am Assoc Cancer Res* **38:** 1087, 1997.
40. van der Laan BFAM, Jansen G, Kathmann GAM, Westerhof GR, Schornagel JH and Hordijk GJ, *In vitro* activity of novel antifolates against human squamous carcinoma cell lines of the head and neck with inherent resistance to methotrexate. *Int J Cancer* **51:** 909–914, 1992.
41. Galivan J, Rhee MS, Johnson TB, Dilwith R, Nair MG, Bunni M and Priest DG, The role of cellular folates in the enhancement of activity of the thymidylate synthase inhibitor 10-propargyl-5,8-dideazafolate against hepatoma cells *in vitro* by inhibitors of dihydrofolate reductase. *J Biol Chem* **264:** 10685–10692, 1989.
42. Lu K, McGuire JJ, Slocum HK and Rustum YM, Mechanisms of acquired resistance to modulation of 5-fluorouracil by leucovorin in HCT-8 human ileocecal carcinoma cells. *Biochem Pharmacol* **53:** 689–696, 1997.
43. Jansen G, Schornagel JH, Kathmann I, Westerhof GR, Hordijk GJ and van der Laan BFAM, Measurement of folylpolyglutamate synthetase activity in head and neck squamous carcinoma cell lines and clinical samples using a new rapid separation procedure. *Oncol Res* **4:** 299–305, 1992.
44. Braakhuis BJM, Jansen G, Noordhuis P, Kegel A and Peters GJ, Importance of pharmacodynamics in the *in vitro* antiproliferative activity of the antifolates methotrexate and 10-ethyl-10-deazaaminopterin against human head and neck squamous cell carcinoma. *Biochem Pharmacol* **46:** 2155–2161, 1993.
45. Pizzorno G, Chang YM, McGuire JJ and Bertino JR, Inherent resistance of human squamous carcinoma cell lines to methotrexate as a result of decreased polyglutamylation of this drug. *Cancer Res* **49:** 5275–5280, 1989.
46. van der Wilt CL, Cloos J, de Jong M, Pinedo HM and Peters GJ, Screening of colon tumor cells and tissues for folylpolyglutamate synthetase activity. *Oncol Res* **7:** 317–321, 1995.
47. Mendelsohn LG, Gates SB, Habeck LL, Shakelford KA, Worzalla J, Shih C and Grindey GB, The role of dietary folate in modulation of folate receptor expression, folypolyglutamate synthetase activity and the efficacy and toxicity of Lometrexol. *Adv Enzyme Regul* **36:** 365–381, 1996.
48. Priest DG, Doig MT and Mangum M, Response of mouse hepatoma cell methylenetetrahydrofolate polyglutamates to folate deprivation. *Biochim Biophys Acta* **756:** 253–257, 1983.
49. Shane B, Folylpolyglutamate synthesis and role in the regulation of one-carbon metabolism. *Vitam Horm* **45:** 263–335, 1989.
50. Kisliuk RL, Pteroylpolyglutamates. *Mol Cell Biochem* **39:** 331–345, 1981.
51. McGuire JJ and Bertino JR, Enzymatic synthesis and function of folylpolyglutamates. *Mol Cell Biochem* **38** Spec No(Pt 1)**:** 19–48, 1981.
52. Westerhof GR, Schornagel JH, Kathmann I, Jackman AL, Rosowsky A, Forsch RA, Hynes JB, Boyle FT, Peters GJ, Pinedo HM and Jansen G, Carrier- and receptor-mediated transport of folate antagonists targeting folate-dependent enzymes: Correlates of molecular-structure and biological activity. *Mol Pharmacol* **48:** 459–471, 1995.
53. Gates SB, Mendelsohn LG, Shackelford KA, Habeck LL, Kursar JD, Gossett LS, Worzella JF, Shih C and Grindey GB, Characterization of folate receptor from normal and neoplastic murine tissue: Influence of dietary folate on folate receptor expression. *Clin Cancer Res* **2:** 1135–1141, 1996.